

Energy-based Contact Planning under Uncertainty for Robot Air Hockey

Julius Jankowski^{*1,2}, Ante Marić^{*1,2}, Puze Liu^{3,4}, Davide Tateo³, Jan Peters^{3,4,5}, and Sylvain Calinon^{1,2}

Abstract—Planning robot contact often requires reasoning over a horizon to anticipate outcomes, making such planning problems computationally expensive. In this letter, we propose a learning framework for efficient contact planning in real-time subject to uncertain contact dynamics. We implement our approach for the example task of robot air hockey. Based on a learned stochastic model of puck dynamics, we formulate contact planning for shooting actions as a stochastic optimal control problem with a chance constraint on hitting the goal. To achieve online re-planning capabilities, we propose to train an energy-based model to generate optimal shooting plans in real time. The performance of the trained policy is validated in simulation and on a real-robot setup. Furthermore, our approach was tested in a competitive setting as part of the *NeurIPS 2023 Robot Air Hockey Challenge*.

I. INTRODUCTION

Planning and control through non-prehensile contacts is an essential skill for robots to interact with their environment. Model-based approaches enable robots to anticipate the outcome of contact interactions given a candidate action allowing them to find an action with the desired outcome. While model-based planning approaches are shown to be successful at generating contact-rich plans for slow tasks [1], [2], highly dynamic tasks require the agent to regenerate contact plans at a sufficiently high rate for reacting to inherent perturbations. Highly dynamic tasks not requiring reasoning through contacts have historically been used as a testbed for hardware and algorithms in robotics. These tasks include different types of games and sports, such as ball-in-a-cup [3], [4], juggling [5], [6], diabolo [7]. Dynamic tasks involving contacts, such as soccer [8], tennis [9], table tennis [10], [11], and air hockey [12], [13], are typically approached with reinforcement learning methods to off-load the computationally expensive reasoning through contacts to an offline exploration phase. Yet, these tasks have in common that contacts with the ball or puck are instantaneous, i.e. the

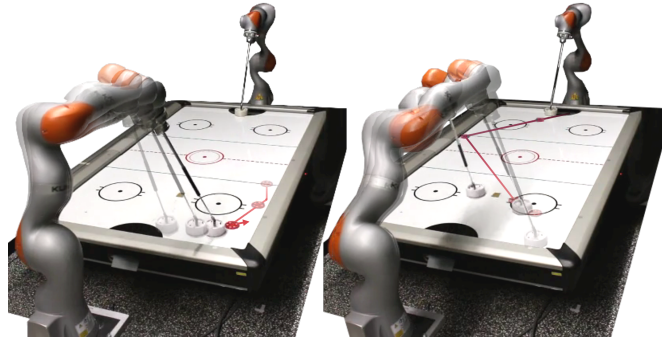


Fig. 1. The proposed control framework enables a robot arm to autonomously play matches of air hockey. First, a learned stochastic model of contact dynamics is used to predict the trajectory of a puck. An energy-based contact planner is then trained to generate agile behavior in real time.

contact happens in a short period of time, resulting in a jump in the state of the object. The reasoning over the contact between the robot and the object of interest can therefore be divided into three segments of the planning horizon: *i*) Moving the robot into contact, *ii*) the contact itself at a single time instance, and *iii*) the passive trajectory of the object after contact.

In this letter, we exploit the separability in the planning horizon by combining a model-based control approach for moving the robot into contact with a learning-based approach for planning the next best contact that results in the desired trajectory of the object. Towards this end, we learn a mixture of linear-Gaussian modes for modeling the object dynamics from data, which allows us to extract a stochastic model for the contact between the robot and the object. Based on the learned model, we train an energy-based contact policy by generating example contacts that are optimal w.r.t. a stochastic optimal control objective offline. During the online phase, we retrieve optimal contact plans from the energy-based policy using derivative-free inference in real time.

In the following, we present our approach in the context of the highly-dynamic game *air hockey*. Fig. 2 illustrates the online control framework that consists of state estimation, the proposed learning-based contact planner (shooting policy), and a subsequent model-based robot controller (MPC). For the robot controller, we use a sampling-based model-predictive controller [14] that enforces the execution of the contact plan while respecting safety constraints such as collision avoidance with the walls. We summarize our key scientific contributions as follows:

- We present an approach for learning the parameters of a stochastic model for discontinuous contact dynamics as a mixture of linear-Gaussian modes.

This work was supported by the Swiss National Science Foundation (SNSF) through the CODIMAN project, by the State Secretariat for Education, Research and Innovation in Switzerland for participation in the European Commission's Horizon Europe Program through the INTELLIMAN project (<https://intelliman-project.eu/>, HORIZON-CL4-Digital-Emerging Grant 101070136) and the SESTOSENSE project (<http://sestosenso.eu/>, HORIZON-CL4-Digital-Emerging Grant 101070310), by the China Scholarship Council (Grant 201908080039) and by the German Federal Ministry of Education and Research (BMBF) through the KIARA project (Grant 13N16274).

* Equal contribution

¹ Idiap Research Institute, Martigny, Switzerland

² École Polytechnique Fédérale de Lausanne (EPFL), Switzerland

³ Intelligent Autonomous Systems, TU Darmstadt, Germany

⁴ German Research Center for AI (DFKI)

⁵ Centre for Cognitive Science, Hessian.AI

Corresponding authors: ante.marić@idiap.ch; julius.jankowski@idiap.ch

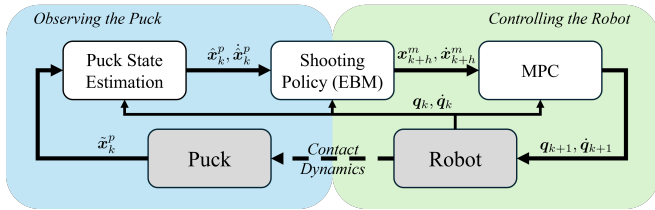


Fig. 2. Overview of the interplay between puck state estimation \bullet and robot control \bullet in our framework for agile robot air hockey. The contact planner uses the estimated puck state to predict the puck trajectory based on the learned model. It subsequently plans a shooting angle that is used to construct an optimal control objective solved within a model-predictive controller. All modules are updated at a control rate of 50 Hz.

- We formulate the planning of contacts as a chance-constrained stochastic optimal control problem.
- We propose an approach for training an energy-based model to capture the optimal policy according to the chance-constrained stochastic optimal control problem.

Our approach is experimentally validated in a dynamic air hockey shooting task with comparisons to control-based and reinforcement learning baselines. We additionally deploy our framework in a competitive setting as part of the NeurIPS 2023 Robot Air Hockey Challenge (see Fig. 1). Our framework outperforms all other approaches in real-robot matches, establishing a new state-of-the-art in robot air hockey.

II. RELATED WORK

The air hockey task has been part of the robotics literature for a long time [15]. One of the first works using the air hockey task as a benchmark focused on skill learning of a humanoid robot [16], [17]. In more recent years, this benchmark has been used in combination with planar robots due to high-speed motion requirements [18], [19], [20], [21], and the possibility of adapting the playing style against the opponent [22]. This benchmark has been recently extended to the cobot setting, where a 7-DoF robotic arm controls the mallet and maintains the table surface while striking [23], [24], [25].

Another use of the robot air hockey setting is as a testbed for learning algorithms. In [26], deep reinforcement learning techniques are used to learn on planar robots, while in [12], both the planar 3-DoF and the 7-DoF cobot air hockey tasks are used to learn control policies in simulation. More recent techniques directly use the real 7-DoF air hockey setting as a testbed for learning algorithms: in [27], the authors use learning-to-plan techniques to generate air hockey hitting trajectories in the real-world setting, while [13], this task is used to perform real-world reinforcement learning.

In general, existing solutions to the robot air hockey problem can be categorized in two main directions: learning-based approaches [17], [26], [13], and control-based approaches [21], [23], [24]. Generally speaking, pure control-based approaches lead to better and faster solutions than learning-based methods but require considerable efforts in engineering and model identification, and are particularly challenging to implement to run at real-time control rates. Instead, pure learning-based approaches obtain a worse-quality

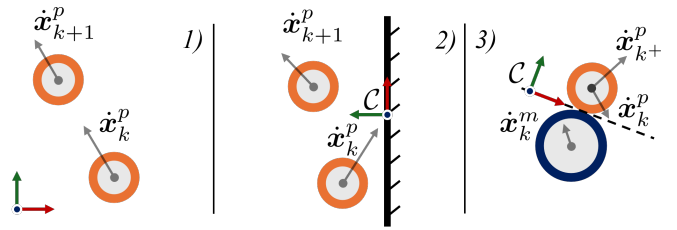


Fig. 3. Illustration of three modes of the puck dynamics that are parameterized as linear-Gaussian models. Mode 1) captures the dynamics of the puck \bullet when floating on the surface of the table. Mode 2) captures collisions between puck and walls. Mode 3) models collisions between puck and the mallet \bullet in a contact-aligned frame C . The parameters for the nominal dynamics and the corresponding uncertainty are learned from data.

solution but make it possible to obtain more robust behaviors by relying on domain randomization and fine-tuning on the real platform. In this letter, we aim to combine the advantages of learning-based and control-based approaches. We exploit the optimality of control-based approaches for controlling the robot without consideration of the puck and exploit the robustness and flexibility of learning-based approaches to efficiently generate plans for the contact between the robot and the puck to maximize the chance of scoring.

III. LEARNING STOCHASTIC CONTACT MODELS

Planning and controlling the contacts of the robot with the puck requires the anticipation of puck trajectories. To enable this, we learn a simplified stochastic model of the puck dynamics for *i*) estimating the current state of the puck online, *ii*) predicting the trajectory of the puck online, and *iii*) solving a stochastic optimal control problem to plan the next best contact between the robot and the puck.

A. Mixture of linear-Gaussian Contact Dynamics

Suppose that $x_k^p \in \mathbb{R}^2$ is the position of the puck w.r.t. the surface of the air hockey table at time step k . The robot interacts with the puck by making contact with its mallet, i.e. the circular part of the robot's end-effector. The position of the mallet is denoted with $x_k^m \in \mathbb{R}^2$ w.r.t. the surface of the air hockey table. We assume that the robot arm is controlled such that the mallet maintains contact with the table at all times. In order to efficiently perform rollouts of the puck dynamics, we impose a piecewise-linear structure on the model. Fig. 3 illustrates the three modes that we present in the following: 1) *Floating*, 2) *Puck-Wall Collision*, and 3) *Puck-Mallet Collision*. To account for modeling errors introduced through the piecewise-linear structure, we model each mode as a conditional Gaussian distribution, resulting in a mixture of linear-Gaussian contact dynamics. In the following, we present the individual modes and their respective parameters that are learned subsequently. Note that the learnable parameters define the stochastic prediction of the puck velocity, while the one-step prediction of the position is derived from numerical integration and is deterministic.

1) *Floating*: The first mode captures the dynamics of the puck when it is freely floating on the table and is not in collision with the wall or mallet. The prediction of the puck velocity is modeled stochastically with

$$\Pr_1(\dot{\mathbf{x}}_{k+1}^p | \dot{\mathbf{x}}_k^p) = \mathcal{N}(\Theta_1 \dot{\mathbf{x}}_k^p + \theta_1, \Sigma_1), \quad (1)$$

where $\Theta_1, \theta_1, \Sigma_1$ are parameters of the conditional Gaussian distribution.

2) *Puck-Wall Collision*: The second mode models the dynamics of the puck reflecting against the wall. The prediction of the velocity is modeled in a coordinate system \mathcal{C} that is aligned with the contact surface of the corresponding wall. The one-step prediction of the puck velocity is modeled with

$$\Pr_2({}^c\dot{\mathbf{x}}_{k+1}^p | {}^c\dot{\mathbf{x}}_k^p) = \mathcal{N}(\Theta_2 {}^c\dot{\mathbf{x}}_k^p + \theta_2, \Sigma_2), \quad (2)$$

where ${}^c\dot{\mathbf{x}}^p$ is the puck velocity in the contact-aligned coordinate system. $\Theta_2, \theta_2, \Sigma_2$ are parameters of this mode.

3) *Puck-Mallet Collision*: As a third mode, we model the interaction between the puck and the mallet as a collision in which the velocity of the puck changes instantaneously at the time of contact. We also model this mode using a conditional Gaussian distribution

$$\Pr_3({}^c\dot{\mathbf{x}}_{k+}^p | {}^c\dot{\mathbf{x}}_{k-}^p, {}^c\dot{\mathbf{x}}_k^m) = \mathcal{N}(\Theta_3^p {}^c\dot{\mathbf{x}}_{k-}^p + \Theta_3^m {}^c\dot{\mathbf{x}}_k^m + \theta_3, \Sigma_3). \quad (3)$$

The velocities of the puck ${}^c\dot{\mathbf{x}}^p$ and of the mallet ${}^c\dot{\mathbf{x}}^m$, respectively, are expressed in the contact-aligned coordinate system \mathcal{C} . The index k^+ corresponds to time step k after applying the collision model, while k^- describes the instant right before the collision. The model parameters for the third mode are $\Theta_3^p, \Theta_3^m, \theta_3, \Sigma_3$.

B. Learning Model Parameters from Data

Given recorded trajectories of the puck and the mallet, the data is fragmented into consecutive puck velocity pairs together with the mallet velocity, i.e. $\dot{\mathbf{x}}_k^p, \dot{\mathbf{x}}_{k+1}^p, \dot{\mathbf{x}}_k^m$, and the corresponding mode is assigned to each data sample. As a result, we assume to obtain a dataset $\{\mathbf{y}_{i,n}, \boldsymbol{\xi}_{i,n}\}_{n=0}^{N_i}$ for each mode i , where $\mathbf{y}_{i,n}$ is the n -th velocity prediction sample for mode i , e.g. $\mathbf{y}_1 = \dot{\mathbf{x}}_{k+1}^p$, and $\boldsymbol{\xi}_{i,n}$ is the n -th prediction condition sample for mode i , e.g. $\boldsymbol{\xi}_1 = \dot{\mathbf{x}}_k^p$. To learn the parameters of the model, we fit a Gaussian distribution to the dataset for each mode modeling the joint probability distribution of prediction and condition with

$$\Pr_i(\mathbf{y}_i, \boldsymbol{\xi}_i) = \mathcal{N}\left(\begin{pmatrix} \boldsymbol{\mu}_{\mathbf{y}_i} \\ \boldsymbol{\mu}_{\boldsymbol{\xi}_i} \end{pmatrix}, \begin{pmatrix} \boldsymbol{\Sigma}_{\mathbf{y}_i} & \boldsymbol{\Sigma}_{\mathbf{y}_i \boldsymbol{\xi}_i} \\ \boldsymbol{\Sigma}_{\mathbf{y}_i \boldsymbol{\xi}_i}^\top & \boldsymbol{\Sigma}_{\boldsymbol{\xi}_i} \end{pmatrix}\right). \quad (4)$$

Given the parameters of the joint probability distribution, the parameters of the linear-Gaussian models can be computed by conditioning the probability distribution on the input $\boldsymbol{\xi}$. The parameters are thus given by

$$\begin{aligned} \Theta_i &= \boldsymbol{\Sigma}_{\mathbf{y}_i \boldsymbol{\xi}_i} \boldsymbol{\Sigma}_{\boldsymbol{\xi}_i}^{-1}, \\ \theta_i &= \boldsymbol{\mu}_{\mathbf{y}_i} - \boldsymbol{\Sigma}_{\mathbf{y}_i \boldsymbol{\xi}_i} \boldsymbol{\Sigma}_{\boldsymbol{\xi}_i}^{-1} \boldsymbol{\mu}_{\boldsymbol{\xi}_i}, \\ \Sigma_i &= \boldsymbol{\Sigma}_{\mathbf{y}_i} - \boldsymbol{\Sigma}_{\mathbf{y}_i \boldsymbol{\xi}_i} \boldsymbol{\Sigma}_{\boldsymbol{\xi}_i}^{-1} \boldsymbol{\Sigma}_{\mathbf{y}_i \boldsymbol{\xi}_i}^\top. \end{aligned} \quad (5)$$

C. Piecewise-linear Kalman Filtering

The learned linear-Gaussian models allow us to update the estimated state of the puck using the Kalman filter. As a result, an estimate of the puck state at time step k , i.e. $\hat{\mathbf{s}}_k = (\hat{\mathbf{x}}_k^p, \dot{\hat{\mathbf{x}}}_k^p)^\top$, is obtained based on a noisy measurement of the puck position $\tilde{\mathbf{x}}_k^p$. For this, the mode of the dynamics is detected at each time step such that the corresponding parameters are used within the Kalman filter update. The parameters are translated into linear-Gaussian state-space dynamics, i.e.

$$\Pr_i(\mathbf{s}_{k+1} | \mathbf{s}_k) = \mathcal{N}(\mathbf{A}_i \mathbf{s}_k + \mathbf{b}_i, \mathbf{Q}_i), \quad (6)$$

with system parameters $\mathbf{A}_i, \mathbf{b}_i$ and process noise covariance matrix \mathbf{Q}_i computed with

$$\mathbf{A}_i = \begin{pmatrix} \mathbf{A}_{i,xx} & \mathbf{A}_{i,x\dot{x}} \\ \mathbf{0} & \Theta_i \end{pmatrix}; \mathbf{b}_i = \begin{pmatrix} \mathbf{0} \\ \theta_i \end{pmatrix}; \mathbf{Q}_i = \begin{pmatrix} \mathbf{0} & \mathbf{0} \\ \mathbf{0} & \Sigma_i \end{pmatrix}. \quad (7)$$

Here, the model parameters $\mathbf{A}_{i,xx}, \mathbf{A}_{i,x\dot{x}}$ determine the prediction of the puck position at the next time step given the current puck position and velocity. These parameters are derived using numerical integration and are constant.

D. Probability of Hitting the Goal

For the robot to anticipate whether a candidate shot may lead to scoring a goal, we predict the probability of hitting the goal based on the learned linear-Gaussian puck dynamics. Note that the probability of hitting the goal does not account for a defending opponent. Without loss of generality, suppose that the collision between mallet and puck happens at $k = 0$. Given the puck state at the time of collision $\hat{\mathbf{s}}_{0-}$ and the corresponding mallet state $\mathbf{x}_0^m, \dot{\mathbf{x}}_0^m$, the expected puck velocity after the collision is computed as defined in (3), resulting in the expected puck state $\hat{\mathbf{s}}_{0+}$. By rolling out the discretized stochastic model with

$$\begin{aligned} \hat{\mathbf{s}}_{k+1} &= \mathbf{A}_{i_k} \hat{\mathbf{s}}_k + \mathbf{b}_{i_k}, \\ \mathbf{P}_{k+1} &= \mathbf{A}_{i_k} \mathbf{P}_k \mathbf{A}_{i_k}^\top + \mathbf{Q}_{i_k}, \end{aligned} \quad (8)$$

a Gaussian distribution of puck states, i.e. $\mathbf{s}_k \sim \mathcal{N}(\hat{\mathbf{s}}_k, \mathbf{P}_k)$ is obtained for each time step $k > 0$. The rollout is initialized with $\hat{\mathbf{s}}_0 = \hat{\mathbf{s}}_{0+}$ and $\mathbf{P}_0 = \mathbf{Q}_3$, exploiting the separated stochastic model of collisions between mallet and puck.

To evaluate the probability of scoring a goal, we perform the stochastic rollout as defined in (8) until the expected puck position $\hat{\mathbf{x}}_k^p$ crosses the goal line. We denote this time step with k_{goal} . In the following, we denote the probability of scoring a goal, i.e. $G = 1$, given a puck position as a Bernoulli distribution with

$$\Pr(G = 1 | \mathbf{x}_k^p) = \begin{cases} 1, & \text{if } \mathbf{x}_k^p \in \mathcal{X}_{\text{goal}} \\ 0, & \text{else.} \end{cases} \quad (9)$$

The subset in puck position space $\mathcal{X}_{\text{goal}}$ represents the goal region. Consequently, we can compute the probability of scoring a goal given the initial conditions of a shot by marginalizing over the puck position at time step k_{goal} with

$$\Pr(G = 1 | \hat{\mathbf{s}}_{0-}, \mathbf{x}_0^m, \dot{\mathbf{x}}_0^m) = \int_{\mathcal{X}_{\text{goal}}} \Pr(\mathbf{x}_{k_{\text{goal}}}^p) d\mathbf{x}_{k_{\text{goal}}}^p. \quad (10)$$

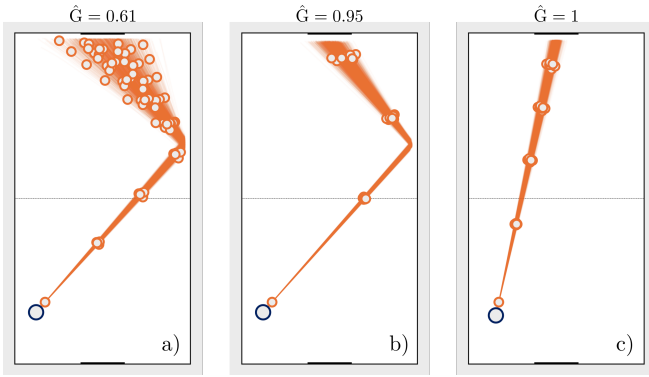


Fig. 4. A qualitative comparison of the probability of hitting the goal \hat{G} for different shooting angles and shooting speeds. The shooting angles are indicated by the mallet position \bullet w.r.t. the puck position \circ at the time of contact. The shooting speed, i.e. the speed of the mallet at the time of contact, is $1.2 \frac{\text{m}}{\text{s}}$ for a) and c), while the shooting speed is $2 \frac{\text{m}}{\text{s}}$ for b).

We compute the probability in (10) using Monte-Carlo approximation by sampling N_G puck positions from the Gaussian distribution at prediction time step k_{goal} and counting the number of samples that would hit the goal

$$\Pr(G = 1 | \hat{s}_{0-}, \mathbf{x}_0^m, \dot{\mathbf{x}}_0^m) \approx \frac{1}{N_G} \sum_{n=1}^{N_G} \Pr(G = 1 | \mathbf{x}_{k_{\text{goal}}, n}^p), \quad (11)$$

with $\mathbf{x}_{k_{\text{goal}}, n}^p \sim \Pr(\mathbf{x}_{k_{\text{goal}}}^p)$. In the following, we denote the approximated probability of hitting the goal, corresponding to the right-hand side of (11), with \hat{G} .

Fig. 4 illustrates stochastic rollouts for various initial conditions of a shot. Evaluating \hat{G} as defined in (11), we observe that those initial conditions have a significant effect even if the expected puck trajectory hits the center of the goal for all conditions. Fast shots (Fig. 4-b) accumulate less uncertainty compared to slow shots (Fig. 4-a) due to the fact that the modeled process noise is constant over time. Compared to bank shots, direct shots accumulate less uncertainty during rollout since collisions with a wall add significant process noise (Fig. 4-c).

IV. FAST CONTACT PLANNING UNDER UNCERTAINTY

The learned dynamics model enables the prediction of uncertain puck trajectories for contact planning. In particular, we aim to find contact states of the mallet that result in desired puck trajectories after contact. The proposed contact planning module is based on stochastic optimal control, optimizing for the mallet state at contact. We combine the optimization of the contact state with a model-based robot controller that drives the robot to the desired contact state at the desired contact time (cf. Fig. 2).

A. Stochastic Optimal Control for Shooting

Given the desired time of contact and the corresponding estimate of the puck state s_{0-} at that time, we pose contact planning for shooting as a stochastic optimal control problem searching for the mallet state $\mathbf{x}_0^m, \dot{\mathbf{x}}_0^m$ at the time of contact.

For this, we aim to maximize a tradeoff between the probability of hitting the goal \hat{G} and the expected puck speed v_{puck} at the goal line. The expected puck speed is computed as the norm of the mean puck velocity at k_{goal} according to Sec. III-D. While the probability of hitting the goal \hat{G} does not account for a defending opponent, we use the speed of the puck as a measure of the difficulty of defending against the shot. The stochastic optimal control problem is given as

$$\begin{aligned} \max_{\mathbf{x}_0^m, \dot{\mathbf{x}}_0^m} \quad & \lambda_1 \hat{G} + \lambda_2 v_{\text{puck}} \\ \text{s.t.} \quad & \hat{G} > \beta, \end{aligned} \quad (12)$$

where we deploy an additional chance constraint to enforce the probability of hitting the goal to be higher than a threshold β based on the learned stochastic model. The weights λ_1 and λ_2 are used for tuning for the desired behavior. Based on the qualitative comparison illustrated in Fig. 4, we expect that solely optimizing for the probability of hitting the goal results only in direct shots, as bank shots induce uncertainty. Yet, due to the kinematics of the robot, the puck speed may be increased with bank shots. Thus, depending on the puck state, the tuned objective can produce both straight shots and bank shots, increasing the chances of scoring.

B. Shooting Angle as Reduced Action Space

The goal of the shooting policy is to find the optimal mallet state at the time of contact, i.e. \mathbf{x}_0^m and $\dot{\mathbf{x}}_0^m$, respectively. Due to the underlying contact geometry and constraints, for a given puck position $\hat{\mathbf{x}}_0^p$ we parameterize the mallet position as a shooting angle $u \in \mathcal{U}$ between the mallet and puck. Note that a shooting angle of $u = 0$ corresponds to a straight shot that is parallel to the side walls of the table. We reduce the dimensionality of the action space further by imposing two heuristic constraints on the mallet velocity $\dot{\mathbf{x}}_0^m$: *i)* The mallet velocity at the time of contact aligns with the shooting angle, such that $\dot{\mathbf{x}}_0^m = v(\cos u, \sin u)^\top$ with scalar velocity $v > 0$ encoding the norm of the mallet velocity. While this constraint excludes shooting angles that are not aligned with the mallet velocity, it enforces maximum transmission of kinetic energy from the robot to the puck. *ii)* We impose that the norm of the mallet velocity is maximal given a shooting configuration \mathbf{q}_0 of the robot and velocity limits $\dot{\mathbf{Q}}$ of the joints of the robot, such that

$$\begin{aligned} v^* &= \max v \\ \text{s.t.} \quad & v \mathbf{e}_u = \mathbf{J}(\mathbf{q}_0) \dot{\mathbf{q}}_0, \\ & \dot{\mathbf{q}}_0 \in \dot{\mathbf{Q}}. \end{aligned} \quad (13)$$

Note that the unit vector $\mathbf{e}_u \in \mathbb{R}^3$ encodes the shooting direction including zero contribution in the z-direction. Accordingly, $\mathbf{J}(\mathbf{q}_0) \in \mathbb{R}^{3 \times n_{\text{dof}}}$ corresponds to the Jacobian w.r.t. the Cartesian position of the mallet.

As a result, the shooting angle u is the action that we optimize for. With the imposed constraints, a shooting angle uniquely maps to a mallet state at the time of contact. Thus, in the following, we denote the probability of scoring a goal as a function of the shooting angle with $\Pr(G = 1 | \hat{s}_{0-}, u)$.

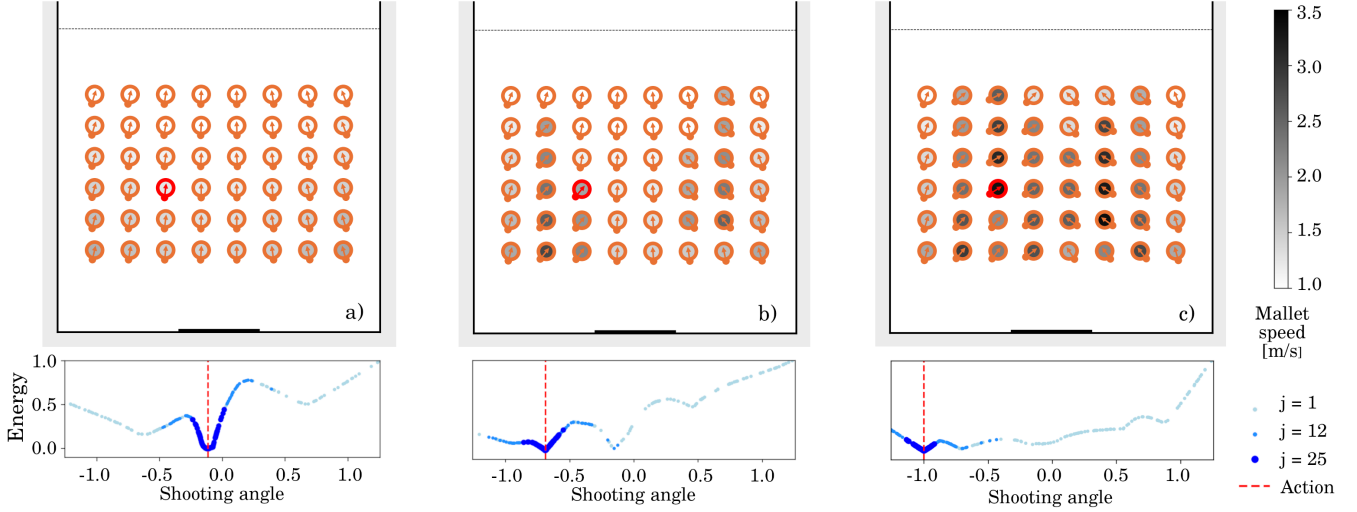


Fig. 5. Examples of differently tuned shooting plans and corresponding energy landscapes. Shooting direction and mallet speed are displayed for varying initial puck positions. Instance a) evaluates only scoring probability ($\lambda_1 = 1$, $\lambda_2 = 0$, $\beta = 0.5$); b) adds additional weight on expected puck speed at the goal line ($\lambda_1 = 1$, $\lambda_2 = 0.2$, $\beta = 0.5$); c) evaluates only the expected puck speed at the goal line ($\lambda_1 = 0$, $\lambda_2 = 1$, $\beta = 0.5$). The energy landscape and sampling process at timesteps $j \in \{1, 12, 25\}$ are visualized for an example shot denoted in red. All pucks are static at $j = 0$.

C. Training an Energy-based Shooting Policy

The long-horizon predictions required to plan shooting actions make it difficult to operate at a rate that is sufficient for agile behavior. We address this challenge by training an energy-based model to reproduce the solutions to the stochastic optimal shooting problem (12) in real-time. Due to implicit policy representation, energy-based models are particularly well-suited for multi-modal solution spaces [28]. In the case of shooting, different modes of the policy include straight shots, single bank shots, and double bank shots.

We train the energy-based model by solving the computationally expensive shooting angle optimization offline and using the results as training data. Namely, we first generate a dataset of shooting angles for N different scenarios, i.e. puck states at the time of contact $\{\mathbf{s}_i\}_{i=1}^N$. Due to the one-dimensional parametrization of the action space, we efficiently explore the space of shooting angles for each initial puck state by sampling M candidate shooting angles $\{u_i^j\}_{j=1}^M$. We subsequently compute the stochastic rollout of the puck trajectory as presented in Sec. III-D and evaluate the objective and chance constraint from (12). The best-performing sample \hat{u}_i is then used as a positive example for training, and the remaining $M - 1$ samples as negative counter-examples. We finally obtain a dataset of $M \times N$ state-action pairs $\{\mathbf{s}_i, \hat{u}_i, \{u_i^j\}_{j=1}^{M-1}\}_{i=1}^N$ and train the energy model $E_\theta(\mathbf{s}, u)$ using an InfoNCE-style [29] loss

$$\mathcal{L}_{\text{InfoNCE}} = \sum_{i=1}^N -\log \left(\tilde{p}_\theta(\hat{u}_i | \mathbf{s}_i, \{u_i^j\}_{j=1}^{M-1}) \right), \quad (14)$$

where $\tilde{p}_\theta(\hat{u}_i | \mathbf{s}_i, \{u_i^j\}_{j=1}^{M-1})$ represents a likelihood with

$$\tilde{p}_\theta(\hat{u}_i | \mathbf{s}_i, \{u_i^j\}_{j=1}^{M-1}) = \frac{e^{-E_\theta(\mathbf{s}_i, \hat{u}_i)}}{e^{-E_\theta(\mathbf{s}_i, \hat{u}_i)} + \sum_{j=1}^{M-1} e^{-E_\theta(\mathbf{s}_i, u_i^j)}}. \quad (15)$$

Algorithm 1: Shooting policy (EBM inference)

Input: Puck state $\hat{\mathbf{s}}_{0-}$, variance σ , samples $\{\tilde{p}_i, \tilde{u}_i\}_{i=1}^N$

Output: Shooting angle \hat{u} , new samples $\{\tilde{p}_i, \tilde{u}_i\}_{i=1}^N$

$\{\tilde{u}_i\}_{i=1}^N \leftarrow \sim \text{Multinomial}(N, \{\tilde{p}_i\}_{i=1}^N, \{\tilde{u}_i\}_{i=1}^N)$

$\{\tilde{u}_i\}_{i=1}^N \leftarrow \{\tilde{u}_i\}_{i=1}^N + \sim \mathcal{N}(0, \sigma)$

$\{\tilde{u}_i\}_{i=1}^N \leftarrow \text{clip} \{\tilde{u}_i\}_{i=1}^N \text{ to } \mathcal{U}$

$\{E_i\}_{i=1}^N \leftarrow \{E_\theta(\hat{\mathbf{s}}_{0-}, \tilde{u}_i)\}_{i=1}^N$

$\{\tilde{p}_i\}_{i=1}^N \leftarrow \text{softmax}(-\{E_i\}_{i=1}^N)$

$\hat{u} \leftarrow \text{argmax}(\{\tilde{p}_i\}, \{\tilde{u}_i\})$

The described loss function reduces energy $E_\theta(\mathbf{s}, u)$ for shooting angles that solve the optimization problem in (12), while increasing the energy of non-optimal shooting angles. Once the model is trained, this allows us to infer optimal shooting angles using sampling-based optimization.

D. Online Inference with Warm-Starting

To solve (12) given the estimated puck state $\hat{\mathbf{s}}_{0-}$, we search for the state-action pair that minimizes energy, i.e.

$$\hat{u} = \arg \min_{u \in \mathcal{U}} E_\theta(\hat{\mathbf{s}}_{0-}, u). \quad (16)$$

For real-time optimization, we leverage direct access to the learned energy landscape of the EBM by executing sampling iterations concurrently with other components of the control loop. This allows us to simultaneously refine contact plans as trajectories are being executed on the robot. The online retrieval of optimal shooting angles is based on the derivative-free optimization procedures used in [28]. As in the offline scenario, we initiate an online shooting action by uniformly sampling N candidate actions. Based on the corresponding energies, candidates are resampled with replacement to warm-start optimization at each following

timestep. To converge towards a solution with minimum implicit energy, reductions to the sampling scale σ are applied at each timestep, keeping the optimal contact angle \hat{u} as a reference for the mid-level trajectory planner. A full iteration of the EBM optimization is outlined in Alg. 1. We observe that the learned energy models and utilized optimization procedure efficiently retrieve multimodal contact plans to produce desired behaviors, as shown in Fig. 5.

V. EXPERIMENTAL EVALUATION

This section details the simulated and real-world experiments used to validate our approach in an online contact planning setting. We evaluate the shooting performance of a robot arm controlled by our framework and compare it against state-of-the-art approaches for robot air hockey.

A. Implementation Details

1) *Data Collection for Puck Dynamics:* We use data collected in a physics-based simulator to learn model parameters of puck dynamics as presented in Sec. III. One set of data is collected by randomly moving the robot’s end-effector into contact with the puck and the other set of data is collected without moving the robot and by initializing the puck with a high random velocity. In total, the training set consists of 100 episodes with 50 time steps each, which corresponds to a total of 100 seconds of observations of the puck dynamics.

2) *EBM Architecture and Training:* The energy-based shooting model consists of a multilayer perceptron with 2 hidden, fully connected layers of 128 neurons each. The model is trained on $N = 3000$ initial puck states, with $M = 100$ action samples. Training required between 500 and 1000 epochs to converge for satisfactory performance using the Adam [30] optimizer with a decaying learning rate.

B. Experimental Setup

The experiment is conducted with a KUKA iiwa14 LBR manipulator equipped with a mallet end-effector that is attached to a passive joint for seamless contact with the table surface. Experiments are carried out in a simulated *MuJoCo* environment and on a real-world setup (cf. Fig. 1) for evaluation of sim2real transfer. We evaluate three instances of the proposed approach by using different parameters for the chance-constrained optimization problem in (12). **Ours #1**: a *conservative* policy that prioritizes accuracy ($\lambda_1 = 1, \lambda_2 = 0, \beta = 0.5$); **Ours #2**: a *balanced* policy that compromises between accuracy and puck speed ($\lambda_1 = 1, \lambda_2 = 0.2, \beta = 0.5$); and **Ours #3**: an *aggressive* policy that prioritizes puck speed ($\lambda_1 = 0, \lambda_2 = 1, \beta = 0.5$). Simulated results are also illustrated in Fig. 5 for initial puck velocities of zero. We compare the three instances of our contact planner with: **CB**, a baseline that utilizes conventional planning and control methods [24]; and **ATACOM**, a reinforcement learning approach for learning a robot policy [12]. Note that the ATACOM policy is trained in simulation and deployed in the physical experiment without additional tuning or retraining.

We perform 100 shots with each policy and report the accuracy score, puck speed at the goal line, and the number

TABLE I
RESULTS OF THE SIMULATED EXPERIMENTS.

	Score	Puck Speed [$\frac{m}{s}$] (mean \pm std.)	Num. Banks (mean)
CB	0.51	0.52 \pm 0.24	0.00
Atacom	0.90	0.55 \pm 0.05	0.00
Ours #1	0.93	1.00 \pm 0.20	0.00
Ours #2	0.80	1.44 \pm 0.63	0.53
Ours #3	0.61	1.97 \pm 0.49	1.13

TABLE II
RESULTS OF THE REAL-WORLD EXPERIMENTS.

	Score	Puck Speed [$\frac{m}{s}$] (mean \pm std.)	Num. Banks (mean)
CB	0.49	1.09 \pm 0.24	0.00
Atacom	0.13	0.66 \pm 0.15	0.31
Ours #1	0.78	1.72 \pm 0.20	0.00
Ours #2	0.60	2.02 \pm 0.35	0.37
Ours #3	0.31	2.37 \pm 0.50	0.90

of bank reflections for successful shots. Each shot is initialized by placing the puck within a grid in front of the robot. Due to imperfect air flow on the air hockey table, the puck moves after release, requiring the controlled robot to adapt for a good shot.

C. Results

Recorded metrics are reported in Table I for the simulated environment and in Table II for the real-world environment. Compared to **CB** and **ATACOM**, we observe that our framework is capable of achieving higher scoring accuracy and significantly higher puck speeds in both environments. It can be seen that different instances of our policy obtain either a high score or high puck speeds according to the corresponding parameters of the stochastic optimal control problem. For example, when compared to **Ours #1**, it can be seen that **Ours #3** compromises scoring accuracy for faster puck speeds and a high number of bank reflections, potentially making the shots more difficult to defend against. The higher number of bank reflections produced by **Ours #3** indicates that the robot kinematics allow for higher shooting speeds when hitting laterally, at the risk of missing the goal due to uncertainty gained with every bank reflection. Note that the score of **Ours #3** is lower than the score chance threshold $\beta = 0.5$ for this instance. This indicates that the learned model either has an error in the nominal dynamics or expects too little uncertainty gain due to bank reflections. We further note a decrease in performance for all agents due to the *sim2real* gap, with **ATACOM** showing the highest sensitivity to transfer as it requires fine-tuning on the real environment. **CB** shows the least decrease in performance, as it is parameterized for the real system. However, note that the shooting trajectory optimization loop of **CB** is slower than required to run at 50 Hz, making it prone to errors due to the puck moving unpredictably during the shooting motion. Additionally, we note higher puck speeds in the real setting for all agents as a result of differences in real and simulated contact dynamics. Examples of physical shots of all approaches can be found in the supplementary video.

VI. CONCLUSION

This letter investigates the combination of learning-based contact planning with model-predictive robot control to achieve reactive robot behavior. We apply the proposed algorithms to the highly dynamic game of air hockey that requires long-horizon prediction and contact planning in real time. We experimentally show that our framework outperforms a purely control-based approach and a purely learning-based approach. Future work will seek to further leverage the sample efficiency of structured dynamics models to better capture the underlying contact dynamics of physical systems from real data. Furthermore, we are interested in investigating combinations of learning-based and model-based control approaches for manipulation tasks that involve more complex contact interactions.

REFERENCES

- [1] T. Pang, H. J. T. Suh, L. Yang, and R. Tedrake, "Global planning for contact-rich manipulation via local smoothing of quasi-dynamic contact models," *IEEE Transactions on Robotics*, vol. 39, no. 6, pp. 4691–4711, 2023.
- [2] J. Jankowski, L. Bruder Müller, N. Hawes, and S. Calinon, "Robust pushing: Exploiting quasi-static belief dynamics and contact-informed optimization," *arXiv preprint arXiv:2404.02795*, 2024.
- [3] M. Kawato, F. Gandolfo, H. Gomi, and Y. Wada, "Teaching by showing in kendama based on optimization principle," in *International Conference on Artificial Neural Networks*, pp. 601–606, Springer, 1994.
- [4] J. Kober and J. Peters, "Policy search for motor primitives in robotics," *Advances in neural information processing systems*, vol. 21, 2008.
- [5] K. Ploeger, M. Lutter, and J. Peters, "High acceleration reinforcement learning for real-world juggling with binary rewards," in *Conference on Robot Learning*, pp. 642–653, PMLR, 2021.
- [6] K. Ploeger and J. Peters, "Controlling the cascade: Kinematic planning for n-ball toss juggling," in *2022 IEEE/RSJ International Conference on Intelligent Robots and Systems (IROS)*, pp. 1139–1144, IEEE, 2022.
- [7] F. von Drigalski, D. Joshi, T. Murooka, K. Tanaka, M. Hamaya, and Y. Ijiri, "An analytical diabolo model for robotic learning and control," in *2021 IEEE International Conference on Robotics and Automation (ICRA)*, pp. 4055–4061, IEEE, 2021.
- [8] T. Haarnoja, B. Moran, G. Lever, S. H. Huang, D. Tirumala, J. Humpalik, M. Wulfmeier, S. Tunyasuvunakool, N. Y. Siegel, R. Hafner, et al., "Learning agile soccer skills for a bipedal robot with deep reinforcement learning," *Science Robotics*, vol. 9, no. 89, p. eadi8022, 2024.
- [9] Z. Zaidi, D. Martin, N. Belles, V. Zakharov, A. Krishna, K. M. Lee, P. Wagstaff, S. Naik, M. Sklar, S. Choi, et al., "Athletic mobile manipulator system for robotic wheelchair tennis," *IEEE Robotics and Automation Letters*, vol. 8, no. 4, pp. 2245–2252, 2023.
- [10] K. Mülling, J. Kober, and J. Peters, "A biomimetic approach to robot table tennis," *Adaptive Behavior*, vol. 19, no. 5, pp. 359–376, 2011.
- [11] D. Büchler, S. Guist, R. Calandra, V. Berenz, B. Schölkopf, and J. Peters, "Learning to play table tennis from scratch using muscular robots," *IEEE Transactions on Robotics*, 2022.
- [12] P. Liu, D. Tateo, H. B. Ammar, and J. Peters, "Robot reinforcement learning on the constraint manifold," in *Conference on Robot Learning*, pp. 1357–1366, PMLR, 2022.
- [13] P. Liu, H. Bou-Ammar, J. Peters, and D. Tateo, "Safe reinforcement learning on the constraint manifold: Theory and applications," *arXiv preprint arXiv:2404.09080*, 2024.
- [14] J. Jankowski, L. Bruder Müller, N. Hawes, and S. Calinon, "Vp-sto: Via-point-based stochastic trajectory optimization for reactive robot behavior," in *2023 IEEE International Conference on Robotics and Automation (ICRA)*, pp. 10125–10131, 2023.
- [15] B. E. Bishop and M. W. Spong, "Vision based control of an air hockey playing robot," *IEEE Control Systems Magazine*, vol. 19, no. 3, 1999.
- [16] D. C. Bentivegna, C. G. Atkeson, and G. Cheng, "Learning tasks from observation and practice," *Robotics and Autonomous Systems*, vol. 47, no. 2-3, pp. 163–169, 2004.
- [17] D. C. Bentivegna, C. G. Atkeson, A. Ude, and G. Cheng, "Learning to act from observation and practice," *International Journal of Humanoid Robotics*, vol. 1, no. 04, pp. 585–611, 2004.
- [18] A. Namiki, S. Matsushita, T. Ozeki, and K. Nonami, "Hierarchical processing architecture for an air-hockey robot system," in *2013 IEEE International Conference on Robotics and Automation*, pp. 1187–1192, IEEE, 2013.
- [19] H. Shimada, Y. Kutsuna, S. Kudoh, and T. Suehiro, "A two-layer tactical system for an air-hockey-playing robot," in *IEEE/RSJ International Conference on Intelligent Robots and Systems (IROS)*, 2017.
- [20] K. Igeta and A. Namiki, "Algorithm for optimizing attack motions for air-hockey robot by two-step look ahead prediction," in *IEEE/SICE International Symposium on System Integration*, pp. 465–470, 2017.
- [21] K. Tadokoro, S. Fukuda, and A. Namiki, "Development of air hockey robot with high-speed vision and high-speed wrist," *Journal of Robotics and Mechatronics*, vol. 34, no. 5, pp. 956–964, 2022.
- [22] K. Igeta and A. Namiki, "A decision-making algorithm for an air-hockey robot that decides actions depending on its opponent player's motions," in *2015 IEEE International Conference on Robotics and Biomimetics (ROBIO)*, pp. 1840–1845, IEEE, 2015.
- [23] A. AlAttar, L. Rouillard, and P. Kormushev, "Autonomous air-hockey playing robot using optimal control and vision-based bayesian tracking," in *International Conference Towards Autonomous Robotic Systems (TAROS)*, 2019.
- [24] P. Liu, D. Tateo, H. Bou-Ammar, and J. Peters, "Efficient and reactive planning for high speed robot air hockey," in *2021 IEEE/RSJ International Conference on Intelligent Robots and Systems (IROS)*, pp. 586–593, IEEE, 2021.
- [25] C. Chuck, C. Qi, M. J. Munje, S. Li, M. Rudolph, C. Shi, S. Agarwal, H. Sikchi, A. Peri, S. Dayal, et al., "Robot air hockey: A manipulation testbed for robot learning with reinforcement learning," *arXiv preprint arXiv:2405.03113*, 2024.
- [26] A. Taitler and N. Shimkin, "Learning control for air hockey striking using deep reinforcement learning," in *International Conference on Control, Artificial Intelligence, Robotics Optimization*, 2017.
- [27] P. Kicki, P. Liu, D. Tateo, H. Bou-Ammar, K. Walas, P. Skrzypczyński, and J. Peters, "Fast kinodynamic planning on the constraint manifold with deep neural networks," *IEEE Transactions on Robotics*, 2023.
- [28] P. Florence, C. Lynch, A. Zeng, O. A. Ramirez, A. Wahid, L. Downs, A. Wong, J. Lee, I. Mordatch, and J. Tompson, "Implicit behavioral cloning," in *Proceedings of the 5th Conference on Robot Learning*, vol. 164 of *Proceedings of Machine Learning Research*, pp. 158–168, 2022.
- [29] A. van den Oord, Y. Li, and O. Vinyals, "Representation learning with contrastive predictive coding," *ArXiv*, vol. abs/1807.03748, 2018.
- [30] D. Kingma and J. Ba, "Adam: A method for stochastic optimization," *International Conference on Learning Representations*, 12 2014.